Multitemporal Spaceborne SAR Data for Change Detection in Urban Areas: A Case Study in Shanghai

Osama Adam and Yifang Ban

Division of Geoinformatics
Department of Urban Planning & Environment
Royal Institute of Technology – KTH
Stockholm, Sweden

KEY WORDS: Change detection, SAR, Minimum-error thresholding, Ratio image, Modified ratio, Urban area

ABSTRACT:

The objective of this research is to perform automatic change detection within urban areas using multitemporal spaceborne SAR data in Shanghai. Two scenes of ENVISAT ASAR C-VV images were acquired in September, 2008 and one scene of ERS-2 SAR C-VV image was acquired in September, 1999. A generalized version of Kittler Illingworth minimum-error thresholding algorithm, that takes into account the non-Gaussianity of SAR images, was tested to automatically classify the SAR ratio image into two classes, change and no change. Two types of comparison operators were performed. First, the conventional ratio image was calculated in a way that only increases in backscatter coefficient are detected. Second, a modified ratio operator that takes into accounts both positive and negative changes was also examined. Various probability density functions such as, Log normal, Generalized Gaussian, Nakagami ratio, and Weibull ratio were tested to model the distribution of the change and no change classes. An iterative refinement of the Log normal model is also applied to improve the resolution of the change map. The preliminary results showed that this unsupervised change detection algorithm is very effective in detecting temporal changes in urban areas using SAR images. The best change detection result was obtained using Log normal model with modified ratio operator at 81.5%, which is over 10% high than that of the other three models tested. The initial findings indicated that change detection accuracy varies depending on how the assumed conditional class density function fits the histograms of change and no change classes.

1. INTRODUCTION

Change detection techniques can be divided into two categories, supervised and unsupervised. Post-classification comparison is the most commonly used supervised change detection technique. This method has two main advantages: i) providing from/to change information and ii) all using multi-source, multi-resolution data. The major disadvantage of this method is the high error probability due to the propagation of individual classification error.

Unsupervised change detections, on the other hand, can be performed with no prior knowledge of the study area. The main drawbacks of this technique are i) providing no change type information, and ii) requiring data from the same or very similar sensors at anniversary or near-anniversary dates.

Unsupervised change detection analysis normally involves two steps. First the multitemporal co-registered images are used to generate a change variable image that accentuates intensity in changed areas. Several operators have been tested among them is the image difference (ID) operator and its extension change vector analysis (CVA), which has been used extensively in the context of optical data. Recently in (Inglada & Mercier, 2007), Kullback-Leibler divergence/distance has also been suggested as a change indicator that measures distance between two probability density functions estimated locally. Regarding SAR data, the existence of multiplicative speckle noise makes the use of ID inappropriate instead image rationing is preferable for generating change variable image, since at least theoretically it has the important property of eliminating speckle noise. The second step is the automatic thresholding of the change variable image. Several thresholding algorithms were proposed including Kittler-Illingworth minimum error thresholding algorithm, Otsu's algorithm, and Wang's algorithm (Melgani & Moser, 2002). The most commonly used algorithm is the Kittler-Illingworth minimum error thresholding algorithm (Kittler & Illingworth, 1986).

Multitemporal SAR images have been increasingly used in change detection studies due to SAR's independent of atmospheric conditions and solar illumination and its unique information content. For examples, Ban & Hu (2007) investigated multitemporal RADARSAT-1 SAR for urban land-cover mapping and change detection in the Greater Toronto Area using a supervised method. Bazi *et al*., (2005), performed unsupervised change detection by generalizing Kittler-Illingworth minimum error thresholding algorithm to account for the non Gaussian distribution of SAR images. Bujor *et al*, (2003) investigated four different type of change variables computed from multitemporal SAR images for the purpose of change detection.

With the launch of ESA's ENVISAT ASAR, Canada's RADARSAT-2 SAR, JAXA's ALOS, PalSAR and DLR's Terra SAR-X, multitemporal SAR data are routinely available worldwide, thus provide an excellent opportunity for change detection studies for many fast growing cities and regions in the world such as Shanghai, where frequent cloud-cover and smog make the acquisition of multi-temporal optical data difficult. Therefore, the objective of this research is to investigate multitemporal, single-frequency, single-polarization ENVISAT ASAR image and ERS-2 SAR image for change detection in Shanghai using unsupervised change detection algorithms. In this study, the conventional ratio operator as well as a modified version of this operator will be used and compared.

2. STUDY AREA AND DATA DESCRIPTION

Shanghai is located in the Yangtze River Delta, Eastern China. This flat and fertile plain is a highly productive agricultural area as well as an area upon which urban growth has rapidly taken place. Shanghai has the largest population (18,542,200 persons in 2007) among all Chinese cities, and the figure is forecasted to 25 million by 2020. Shanghai's significant economic expansion and corresponding high rates of urbanization have brought rapid changes to this megacity's urban spatial structure and greatly increased the amount of stress, in the form of waste and pollutants, on the ecosystem (Zhang & Ban, 2009).

Two scenes of ENVISAT ASAR C-VV images were acquired on 03/09/2008 and 19/09/2008 in order to cover Shanghai area. One scene of ERS-2 SAR image acquired on 07/09/1999, a near-anniversary date, was selected from the archived for change detection.

3. METHODOLOGY

3.1 Image Pre-processing

3.1.1 Orthorectification of SAR data:

A geocoded Landsat image was used as the reference image to register all the SAR images to WGS 84 datum with UTM projection. To remove relief displacement, all SAR images were orthorectified using a satellite orbital model and a SRTM DEM with 90m resolution.

3.1.2 Speckle filtering:

The existence of the multiplicative speckle noise in SAR images, affects the ability of the algorithm to separate change and no change classes. To maximize the discrimination capability between change and no change classes a pre-processing step is required to remove this noise in SAR images. Enhanced Lee filter with window size of 7x7 was used to remove the spackle noise. Experiment results show that two iterations of this filter will produce the best result in terms of the achievable accuracy.

3.2 Unsupervised change detection

3.2.1 Problem formulation:

Let us assume that we have two co-registered multitemporal SAR amplitude images acquired at time t_1 and t_2 respectively:

$$X_1 = \{x_1^{ij}, i:1-n, j:1-m\}$$
$$X_2 = \{x_2^{ij}, i:1-n, j:1-m\} \quad (1)$$

Our purpose is to automatically find areas that have changed over time by comparing these two images on a pixel by pixel basis. For SAR images, the ratio operator is normally used to generate the change image variable since it will eliminate the speckle noise assuming that this noise is multiplicative and reproduced in repeat-pass images. This operator divides in a pixel by pixel basis image X_2 by image X_1 as given in (2).

$$R = \frac{X_2}{X_1} \quad (2)$$
$$\text{Where } R = \left\{ r_{ij} = \frac{x_2^{ij}}{x_1^{ij}}, i:1-n, j:1-m \right\}$$

According to Bujor *et al*, (2003), the ratio operator is suitable when it comes to detecting sharp changes such as those associated with urban areas. Adopting single threshold approach (Moser & Serpico, 2006), equation (2) implies that only pixels went through intensity increase over time will be detected. Those with change characterized by intensity decrease, however, will not be detected by the intended algorithm. The ratio operator in its current form is compatible with the purpose of this study, as we are mainly interested in new built up areas that increase intensity in SAR image due to multi corner reflection of SAR signal (Lillesand *et al*, 2007).

A modified version of the ratio operator is also used in this study. This operator takes into account the relation between the amplitude in first and second date images and produces a ratio that is always greater than or equal to one as shown in (3). This operator turns out to be very effective in identifying changed areas using minimum error thresholding algorithm.

$$\text{For each pixel } x_1^{ij}, x_2^{ij}$$
$$\text{If } x_2^{ij} \geq x_1^{ij} \text{ Then } mr_{ij} = \frac{x_2^{ij}}{x_1^{ij}} \text{ Else } mr_{ij} = \frac{x_1^{ij}}{x_2^{ij}} \quad (3)$$

This operator transfer changed pixels with intensity decrease to the other side of the histogram as changed pixels due to intensity increase. The effect is similar to taking the absolute value of the differenced images. This operator has two important merits over the conventional ratio operator. First it increases the prior probability of change class by adding areas where the amplitude or intensity has decreased. This will also increase the size of the change class sample, and consequently, improve the histogram-based estimation of its conditional density function.

3.2.2 Minimum error thresholding algorithm

Unsupervised change detection can be viewed as a binary classification problem with only two possible states of nature (change and no change). If the prior probabilities and probability density functions of change and no change classes are known in advance, then Bayesian decision rule can be used to threshold the change variable into two possible classes in a way that minimizes the probability of classification error (Duda *et al*, 2001). However, in unsupervised change detection the above mentioned information is neither known nor can be directly estimated as no training data exists.

Kittler & Illingworth, (1986) proposed an algorithm that simultaneously estimates the unknown probabilities and locates an optimum threshold r^* that can be used to classify each pixel in the change image into one of two possible classes as shown in (4) below.

$$\text{If } r_{ij} \leq r^*$$
$$\text{Then } r_{ij} \rightarrow \text{No Change Class}$$
$$\text{Else } r_{ij} \rightarrow \text{Change Class} \quad (4)$$

The statistical properties of the change image generated by applying the ratio operator given in (2) or (3), can be summarized by constructing a normalized histogram h(r) consisting of L quantization level. This histogram is a good approximation of the probability density of the ratio image p(r).

According to total probability theorem this probability density p(r) is the result of the combination of two different populations (change and no change) as shown in (5).

$$p(r) = P_1 p_1(r) + P_2 p_2(r) \tag{5}$$

Where P_1 and P_2 are the unknown prior probabilities of no change and change classes respectively, and $p_1(r)$, $p_2(r)$ are their unknown conditional density functions.

Given an arbitrary selected threshold r_T from all possible threshold values (T range from 1 to L) that divides the histogram into two classes it is possible to use each of these histogram sections to estimate the unknown probabilities. First the prior probabilities can be estimated simply from the normalized histogram using (6).

$$P_1 = \sum_{r=r_1}^{r_T} h(r) \quad \text{and} \quad P_2 = \sum_{r=r_{T+1}}^{r_L} h(r) \tag{6}$$

Histogram fitting techniques can then be used to estimate the unknown conditional density functions parameters assuming that their form is known. As for each possible value of the threshold r_T (T range from 1 to L) there exists a new estimation of the unknown probabilities, Kittler & Illingworth, (1986), suggest selecting the threshold that minimizes the criterion function given in (7).

$$J(r_T) = -\sum_{i=1,2}\left[P_i(r_T).\ln P_i(r_T) + \sum_{r\in i} h(r).\ln p_i(r/r_T) \right] \tag{7}$$

Where [i: 1, 2] refer to the no change and change classes. The threshold that minimizes the criterion function is the one that minimizes the probability of classification error. The r_T appeared in the conditional density function and prior probability is used to emphasize that these are estimated for specific threshold value r_T.

In the original minimum error thresholding algorithm, both classes are assumed to have a Gaussian distribution. For SAR amplitude or intensity images this assumption no longer holds. Considering the fact that the accuracy of the methods depends on how accurate the statistical model fits the data, Moser & Serpico, (2006) suggested three probability density functions that can be used to model the distributions of no change and change classes. In (Bazi *et al*., 2005), a generalized version of the Gaussian model is used to model the logarithm of the intensity ratio image. These models and their parameter's estimation techniques are going to be described in the next section.

3.2.3 Statistical models

3.2.3.1 Log normal distribution: If a random variable is log normally distributed, then it is logarithm is normally distributed (Lindgren, 1968). Similar to Gaussian distribution this model is defined using two parameters as in (8).

$$p(r/\varphi_i, \xi_i^2) = \frac{1}{r\xi_i\sqrt{2\pi}} \exp\left(\frac{-(\ln r - \varphi_i)^2}{2\xi_i^2} \right) \tag{8}$$

Where [i: 1, 2] refer to no change and change classes respectively, φ_i and ξ_i^2 are the first and second order log cumulants defined in (9) for the class's conditional density and r is the random variable.

$$\varphi_i = \frac{\sum_{r\in i} h(r)\ln r}{P_i}$$
$$\xi_i^2 = \frac{\sum_{r\in i} h(r)[\ln r - \varphi_i]^2}{P_i} \tag{9}$$

The log normal distribution has the important property of fitting asymmetrical histogram, which makes it more flexible in modelling the distribution of change and no change classes.

3.2.3.2 Weibull ratio model: assuming each of the multitemporal SAR amplitude images to have a Weibull distribution with the same shape parameter, Moser & Serpico, (2006) developed an expression for the probability density function of the SAR amplitude ratio image (10) that depends onto two parameters.

$$p(r/\eta_i, \lambda_i) = \eta_i \lambda_i^{\eta_i} \frac{r^{\eta_i - 1}}{(\lambda_i^{\eta_i} + r^{\eta_i})^2} \tag{10}$$

Where η_i and λ_i are the distribution parameters and the ratio r should be greater than 0. The unknown model's parameters are estimated using the method of log cumulants which relate the unknowns to the first and second order log cumulants as in (11).

$$\varphi_i = \ln \lambda_i \quad , \quad \xi_i^2 = \frac{2\Psi(1,1)}{\eta_i^2} \tag{11}$$

Where φ_i and ξ_i^2 are the first and second order log cumulants as defined in (9), and $\Psi(,)$ is the digamma function.

Although this development ignores the mathematical correlation between multitemporal amplitude images, this model proved to be useful in describing the class's conditional density function.

3.2.3.3 Nakagami ratio model: similar to Weibull ratio model, this model assumes that, each of the SAR amplitude images is Nakagami distributed with the same equivalent number of looks. Image correlation is ignored for simplicity. The probability density function of this model is given in (12).

$$p_i(r/L_i, \gamma_i) = \frac{2\Gamma(2L_i)}{\Gamma^2(L_i)} \frac{\gamma_i^{L_i} r^{2L_i - 1}}{(\gamma_i + r^2)^{2L_i}} \tag{12}$$

Where L_i, γ_i are the distribution parameters and Γ is Gamma function. The estimation of the model's parameters is performed by solving equations (13) which relate the unknown model's parameters to the first and second order log cumulants given in equation (9).

$$\varphi_i = \frac{\ln \gamma_i}{2} \quad , \quad \xi_i^2 = \frac{\Psi(1, L_i)}{2} \tag{13}$$

3.2.3.4 Generalized Gaussian model: This model is a generalization of the normal distribution model, with one additional parameter that describes the shape. Varying the shape parameter, generalized Gaussian model can represent a large family of symmetrical distributions among which are the Gaussian, Laplacian and uniform distributions. Equation (14) shows the probability density function of the generalized Gaussian model.

$$p(r / \mu_i, \sigma_i^2, \alpha_i) = a_i \exp\left[-(b_i |r - \mu_i|)^{\alpha_i}\right] \tag{14}$$

Where $a_i = \frac{b_i \alpha_i}{2\Gamma(\frac{1}{\alpha_i})}$, $b_i = \frac{1}{\sigma_i}\sqrt{\frac{\Gamma(\frac{3}{\alpha_i})}{\Gamma(\frac{1}{\alpha_i})}}$

Where μ_i and σ_i are the conventional mean and standard deviation, and α_i is the shape parameter. The estimation of the first two parameters is straight forward, while the shape parameter can be estimated by the method described in (Sharifi & Leon-Garcia., 1995).

In this work, this model is not going to be used with logarithm of the ratio of the intensity images as suggested by Bazi *et al*., (2005), but rather with the ratio of the amplitude images and the modified ratio image. In fact, taking the logarithm of the ratio image does not only scale the data, but also change its statistical distributional properties (Inglada & Mercier, 2007).

3.3 Log normal improved solution

When dealing with histogram based estimation of the unknown probability density functions, it is essential to consider two important issues. First the resolution and accuracy of the final change map will depend on the histogram's bins size. The higher the number of bins the smaller is their sizes and the higher the accuracy of the final change map. On the other hand, high number of bins means that a lot of them will be empty, which will degrade the accuracy of the density function estimation.

To overcome these problems, we suggest using an iterative solution to improve the final change map accuracy. This solution is based on the fact that using the correct model, there is a unique natural threshold that divides the change variable into two groups. The first solution is obtained by applying fitting techniques adopted in minimum error thresholding algorithm to the ratio image histogram. This solution will produce two groups of pixels attributed to change and no change classes. Due to the relatively coarse histogram's bin size, these two classes are not pure and each of them contains pixels that should be classified on the other class if the correct threshold was selected. Let us consider the change and no change pixels resulted from the histogram based classification a good but not a perfect training sample for each class. These samples can be used to estimate the conditional density function parameters for each class in addition to their prior probabilities.

Based on Bayesian decision theory (Duda *et al*, 2001), the best threshold is the one that satisfies equation (16) where, the classes are assumed to be log normally distributed with known parameters estimated from the training samples.

$$P_1 p_1(r^* / \varphi_1, \xi_1^2) = P_2 p_2(r^* / \varphi_2, \xi_2^2) \tag{16}$$

The only unknown in (16) is the ratio value r^* that represents the best threshold between change and no change. Plugging equation (8) into (16) and taking the logarithm of both sides, we end up with the second order polynomial shown in equation (17) after some mathematical simplification.

$$a\left[\ln r^*\right]^2 + b\left[\ln r^*\right] + c = 0 \tag{17}$$

Where

$$a = \frac{1}{\xi_1^2} - \frac{1}{\xi_2^2}$$

$$b = -2\left[\frac{\varphi_1}{\xi_1^2} - \frac{\varphi_2}{\xi_2^2}\right]$$

$$c = \left[\frac{\varphi_1^2}{\xi_1^2} - \frac{\varphi_2^2}{\xi_2^2}\right] - 2\log_e \frac{P_1}{P_2} + \log_e \frac{\xi_1^2}{\xi_2^2}$$

The solution r^* of equation (17) provides a better threshold to produce accurate binary change map. This new change and no change classes can then be used to estimate new prior probabilities and conditional density functions and locate a new threshold. The iterative solution continues until the threshold converges to a constant value. The last obtained threshold represents the natural separation between two groups of pixels that represent change and no change. It is important for this approach to converge that the statistical model used represents a perfect fit of the class's distribution, otherwise the solution may not converge. Similar expression can also be developed for Weibull ratio, Nakagami ratio and generalized Gaussian models.

This model presented above is especially useful when the numbers of pixels involved in the analysis are limited, since in this case the histogram will not be accurate in describing the statistical properties of the classes. It is an attempt to approach the solution obtained by manual try and error selection of the optimum threshold.

3.4 Accuracy assessment

To assess the accuracy, two Landsat images acquired in almost similar dates to SAR images, were used. The selection of the ground truth data was done by visual inspection of the Landsat images together with the SAR images.

Three different types of samples were selected for accuracy assessment. The first is a sample of areas that did not change. The second and third group of samples was where a change characterized by backscatter increase and decrease respectively occurred. The selected sample covers small areas in comparison

to the whole image areas. Therefore, the accuracy assessment result should be understood in a relative sense.

4. RESULTS AND ANALYSIS

4.1 Conventional ratio operator

The detected changed areas are shown in yellow in Fig. 1 overlaid in a false colour composite (Red: Date2, Green: Date1, Blue: Date2) for the generalized Gaussian, log normal, Nakagami ratio and Weibull ratio models respectively. Using the conventional ratio operator the algorithm was able to identify many changed areas where the backscatter coefficient has increased.

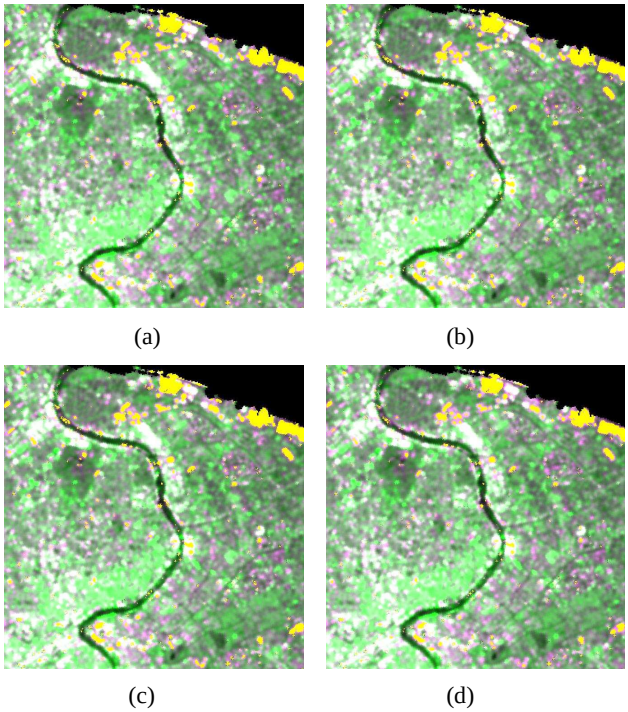

(a) (b)

(c) (d)

Figure 1. Detected changed areas for the first dataset (conventional ratio) in yellow, overlaid in a false colour composite (Red: Date2, Green: Date1, Blue: Date2) (a) Generalized Gaussian. (b) Log normal. (c) Nakagami Ratio. (d) Weibull ratio model.

The first graph in Fig. 2 shows a section of the ratio image histogram corresponding to the no change class. The symmetry and sharp peak of the distribution are evident. Visual inspection of Fig. 1 shows that the results under different models are almost the same with only slight differences. This also confirmed by the fact that under all models except for the Weibull ratio, the thresholds and change percentage shown in the first two rows of Table 1, are almost the same. This similarity is justifiable since all statistical models have the property of fitting sharp, symmetrical distributions. Despite this similarity, visual inspection of the change map and achieved accuracies indicate that the detection results are still not very good.

The analysis of the accuracy assessment results in Table 2 reveals more detailed information. The first row in this table shows the overall detection accuracy including areas where change is characterized by backscatter coefficient decrease. The accuracy in this raw is low since the algorithm missed detect areas with intensity decrease owing to the way in which the ratio image was constructed.

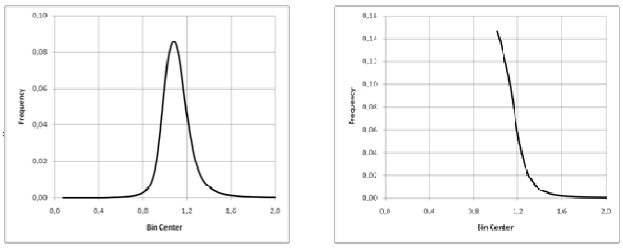

Figure 2. (a) Histogram of the ratio image. (b) Histogram of the modified ratio image.

Models	GG Model	LN Model	NR Model	WR Model
Threshold (Ratio Operator)	1.628	1.604	1.604	1.723
Detected Change % (Ratio Operator)	1.35%	1.48%	1.48%	0.99%
Threshold (Modified Ratio)	1.269	1.395	1.382	1.467
Detected Change % (Modified Ratio)	10.54%	4.62%	4.45%	2.70%

Table 1. Percentage of detected change and selected thresholds for all models using the ratio and modified ratio operator.

Focusing in detection accuracy in areas with intensity increase shown in the fourth raw, the algorithm achieved the highest accuracy under log normal and Nakagami ratio models, whereas its performance with the other two models was slightly lower. The false alarm rates are small and have the same value for the first three models, while for Weibull distribution the false alarm rate was smaller, which is caused by the lower detection accuracy.

Model	GG Model	LN Model	NR Model	WR Model
Detection Accuracy %	66.10	66.90	66.90	63.73
False Alarm %	0.40	0.40	0.40	0.24
Missed Change %	33.90	33.10	33.10	36.27
Intensity Increase Detection %	88.90	89.99	89.99	85.72
Intensity Decrease Detection %	0.00	0.00	0.00	0.00

Table 2. Accuracy achieved using ratio operator

The missed change rates are very high under all models due to two possible reasons. First based on the structure of the ratio operator, the algorithm did not locate any areas with intensity decrease, which is expected. The second reason for the high missed change rates is the fact that the size and consequently, the prior probability of areas with intensity increase are small in comparison to that of no change class. As explained in Duda et al, (2001), the classification will strongly be affected by big differences in prior probabilities of classes. This small size of the change class may also affect the accurate estimation of its conditional density function and as matter of fact the accurate determination of the threshold.

4.2 Modified ratio operator

Using the modified ratio operator the performance of the algorithm improved significantly. Fig. 3 shows the detected

changed areas (using modified ratio operator) in yellow overlaid in a false colour composite (Red: Date2, Green: Date1, Blue: Date2) for generalized Gaussian, log normal, Nakagami ratio and Weibull ratio models respectively. Visually comparing Fig. 3 with Fig. 1 it is clear that with this operator the performance improved significantly and the algorithm identified more areas as change than under the conventional ratio operator. This conclusion is also reflected in accuracy assessment result shown in Table 3.

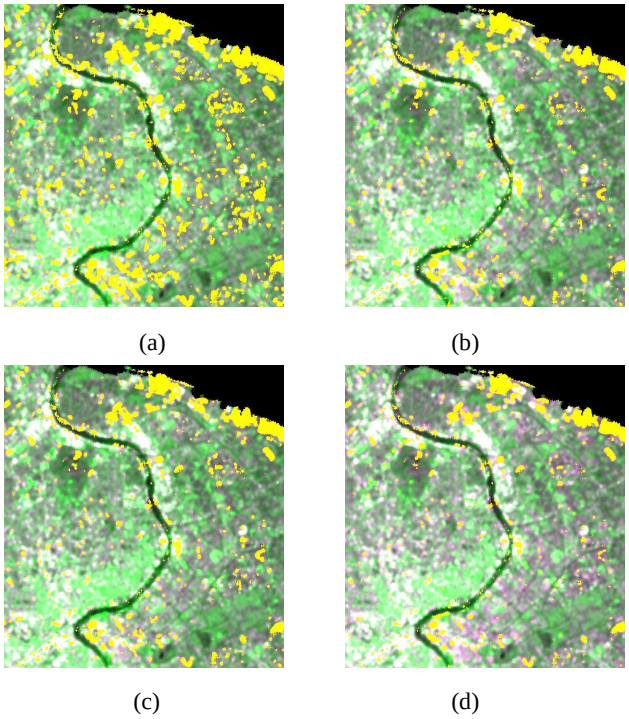

(a) (b)

(c) (d)

Figure 3. Detected changed areas for the first dataset (Modified ratio) in yellow, overlaid in a false colour composite (Red: Date2, Green: Date1, Blue: Date2). (a) Generalized Gaussian. (b) Log normal. (c) Nakagami Ratio. (d) Weibull ratio model.

Using log normal model to describe class's distribution, Fig. 4 show side by side the change detection result for a portion of the second dataset using the ratio image (a), and modified ratio image (b). To the right of the image is Pudong international airport where a lot of new asphaltic manoeuvring areas have been constructed. Under the ratio image, the algorithm missed detects all these new areas. However using the modified ratio image all new manoeuvring areas were correctly identified.

A good improvement in the detection accuracy occurred under all models (Table 3). This improvement occurred because the modified operator increases the prior probability of the change class compared with the conventional operator. Additionally this increase in size of the change class adds more diversity to its sample and enhances the estimation of its conditional density function and consequently, improves the detection accuracy.

The fourth raw in Table 3 shows the improvement in the detection in areas where the intensity has increased. A visual comparison between Fig. 1 and Fig. 3 indicates that the improvement in detection accuracy is even better than the one reflected in Table 3. The slight increase in false alarm rate can easily be attributed to increase in detection accuracy. For the log normal model the missed change rate reduced significantly compared with the first result using the conventional ratio operator. While under other models the high missed change rate stay almost the same.

The second graph of Fig. 2 focuses in the no change class part of the histogram of the modified ratio image. This class's histogram is asymmetric as a result of the way the modified ratio image is calculated. Definitely symmetrical distributions as the generalized Gaussian model are not going to fit this histogram. This is confirmed by the high false alarm rate, high missed change rate, visual inspection and the excessively identified percentage of change under this model shown in the fourth row of Table 1.

The log normal and Nakagami ratio distributions has the ability to fit asymmetrical data. The detection accuracy in intensity increased areas and the false alarm rates for these tow model are the same. However, log normal model outperformed the Nakagami ratio model as it achieved a considerably smaller missed change rate. The Weibull ratio performance is also poor as it underdetermined changed areas.

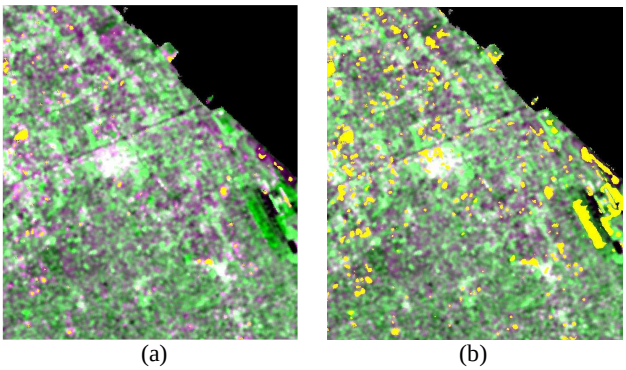

(a) (b)

Figure 4. Detected changed areas for a portion of the second dataset in yellow, overlaid in a false colour composite (Red: Date2, Green: Date1, Blue: Date2). (a) Ratio image and Log normal model. (b) Modified ratio image and log normal model.

Considering the modified ratio operator the algorithm was supposed to be able to discover changed areas with intensity decrease too. Nevertheless, this was not the case as the detection accuracy is zero under all models except for the log normal model which gives a detection accuracy mounted up to 47%. The main reason for this frustrating result is that, the intensity of change as reflected in the change image is very low in areas with backscatter coefficient decrease compared to that in areas with backscatter coefficient increase.

Model	GG Model	LN Model	NR Model	WR Model
Detection Accuracy %	71.28	81.49	69.77	68.91
False Alarm %	4.02	1.05	1.05	0.80
Missed Change %	28.72	18.51	30.23	31.09
Intensity Increase Detection %	95.87	93.50	93.84	92.69
Intensity Decrease Detection %	0.00	46.67	0.00	0.00

Table 3. Accuracy achieved using modified ratio operator

Although the detection of changed areas where the intensity decreased has failed, the algorithm accuracy for the other areas has increased significantly. This improvement is in accordance with the intention of this paper that focuses on new urban areas.

4.3 Log normal improved solution

Using the correct statistical model for change and no change classes, there is a natural unique threshold that separates these two classes. Since it proves to be the best in describing their statistical properties, the log normal was chosen to model change and no change classes for the iterative solution using the modified ratio image.

The first and third graphs in Fig. 5 show the variation in false alarm rate versus iterations for the first and second datasets respectively. The false alarm rate stays constant in the first dataset due to the bigger image size and consequently, the accurate histogram representation. For the second smaller size dataset the histogram is not as representative as in the first one. Therefore, the false alarm reduced dramatically emphasizing the improvement in the separation between the change and no change classes as we iterate.

Graph (b) and (d) in Fig. 5 show the variation of the threshold value versus iterations for the first and second datasets respectively. The graphs show how the threshold quickly converges to constant values after little iterations. This constant value is the natural threshold between the two classes of interest.

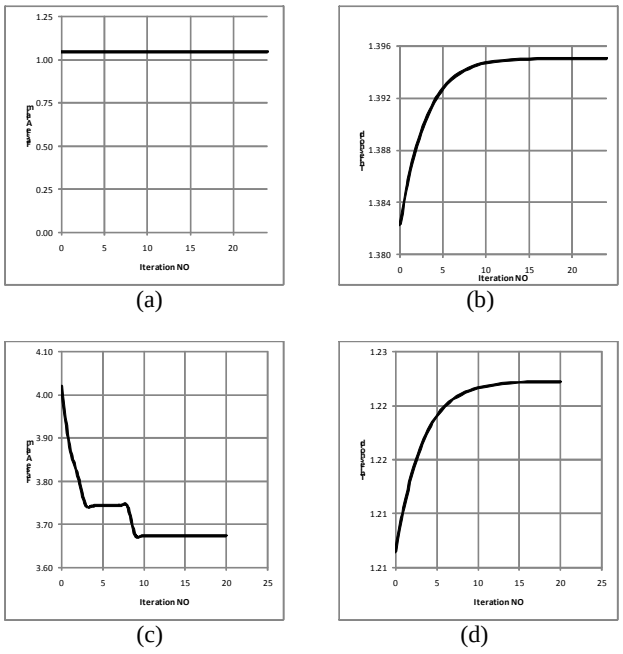

Figure 5, (a) Variation in false alarm and (b) Variation in threshold for the first data set. And the same variation for the second data set in (c) and (d).

Unfortunately, this approach does not converge under other statistical models confirming the suitability of the lognormal model in this particular case study over other models.

5. CONCLUSION

In this paper, the effectiveness of the minimum error thresholding algorithm in identifying changes was evaluated. The preliminary results showed that change detection using Log normal model with modified ratio operator achieved the best accuracy (81.5%) and the areas characterized by backscatter coefficient increase, i.e., from non-builtup to builtup areas, can be detected with 93.5%. Further, the modified ratio approach significantly improved the detection accuracy in intensity increase areas and to some extent in those with intensity decrease.

There are two important issues to be considered when applying unsupervised change detection using minimum error thresholding algorithm. First the statistical models to be used should be able to accurately describe the statistical properties of the class's distribution. In this work, four different statistical models have been tested. Among them the log normal proved to be the best. This does not mean that log normal will perform well in other similar change detection studies. In fact, results reported from similar studies showed that all the above-mentioned models could produce very good results. This large number of proposed models indicates the need of a global model that can fit different type of data with different statistical properties. Another possibility to improve the solution is to use two different models for the change and no change classes instead of using the same single model for both of them.

The second issue is the operator used to compare the multitemporal image and generate the change image. This research showed that the modified ratio operator significantly improved the accuracy of the change detection. A variable that takes into account the local context combined with the global threshold determination of this algorithm could perform even better.

An improved solution that overcomes the limitations of the histogram-based selection of an optimum threshold is also introduced in this paper. This approach requires the probability model to be perfect in representing the distribution of the classes. The quick convergence rate of the threshold to a constant value, confirms the existence of a unique separation value that divides the change image into two classes. Experiment results showed that this approach was more effective with smaller size images and consequently smaller sample size where the histogram is not so accurate in representing the statistical properties of the classes.

REFERENCES

Ban, Y. and H. Hu, 2007. Multitemporal RADARSAT-1 Fine-Beam SAR Data for Land-Cover Mapping and Change Detection. Proceedings, Urban Remote Sensing Joint Event. Paris, France.

Bazi, Y., Bruzzone, L., and Melgani, F., 2005. An unsupervised approach based on the generalized Gaussian model to automatic change detection in multitemporal SAR images. *IEEE Trans on Geoscience and Remote Sensing*, 43(4), pp. 874-887

Bujor, F., Nicolas, J-M., Trouve, E., and Rudant, J-P., 2003. Application of Log-cumulants to change detection in multi-temporal SAR images. *IEEE Trans on Geoscience and Remote Sensing*, 2, pp. 1386-1388.

Duda, R., Hart, P., and Stork, D. 2001. *Pattern classification*. John Wiley & Sons, Inc, China machine press.

Inglada, J. and Mercier, G., 2007. A new statistical similarity measure for change detection in multitemporal SAR images and its extension to multiscale change analysis. *IEEE Trans on Geoscience and Remote Sensing*, 45(5), pp. 1432-1445.

Kittler, J., and Illingworth J., 1986. Minimum error thresholding. *Pattern recognition*, 19(1), pp. 41-47.

Lillesand, T., Kiefer, R., and Chipman, J., 2007. *Remote Sensing and Image Interpretation*. John Wiley & Sons, Inc, USA.

Lindgren, B. W., 1968. *Statistical theory*. Collier-Macmillan, London.

Melgani, F. and Moser, G., 2002. Unsupervised change-detection methods for remote-sensing images. *Optical engineering*, 41(12), pp. 3288-3297.

Moser, G. and Serpico Sebastiano, B., 2006. Generalized Minimum-Error Thresholding for Unsupervised Change Detection from SAR Amplitude Imagery. *IEEE Trans on Geoscience and Remote Sensing*, 44(10), pp. 2972-2982.

Sharifi, K. and Leon-Garcia, A., 1995. Estimation of shape parameter for generalized Gaussian distribution in subband decomposition of video. *IEEE Trans on circuit and systems for video technology*, 5(1), pp. 52-56.

Zhang, Q., Y. Ban., Y. Hu and J. Liu. 2009. The Trajectories of Urban Land and Industrial Land in Shanghai over the Past 30 Years. *Proceedings, Urban Remote Sensing Joint Event.* Shanghai, China.